International Journal of Thermofluid Science and Technology (2023)
Volume 10, Issue 1, Paper No. 100101
https://doi.org/10.36963/IJTST.2023100101
Research Article

Numerical investigation on pressure oscillations in steam condensation from injection of subcooled water

Abdul Quddus[1,*], Ajmal Shah[2], Kamran Rasheed Qureshi[1], Ahmad Tahir[1], Ammar Ahmad[1], Mazhar Iqbal[1] M Khawar Ayub[3] Atif Mehmood[1]

[1]*Department of Mechanical Engineering, Pakistan Institute of Engineering and Applied Sciences, PIEAS, Islamabad, Pakistan.*
[2]*Center for Mathematical Sciences, Pakistan Institute of Engineering and Applied Sciences, PIEAS, Islamabad, Pakistan.*
[3]*Theoretical Physics Division, PINSTECH, Islamabad, Pakistan.*

ATICLE INFO

Received: 21 Nov. 2022;
Received in revised form:
20 Jan. 2023;
Accepted: 22 Jan. 2023;
Published online:
25 Jan. 2023

Keywords:
Pressure oscillations
Dominant frequency
Direct contact condensation
CIWH

ABSTRACT

Steam-water direct contact condensation phenomenon is commonly found in many industries like chemical process industry, nuclear industry etc. In this work the injection of subcooled water into a steam filled pipe has been studied computationally. As a result of steam-water interaction within the pipe the pressure oscillates, which may cause damage to piping system or equipment. The effects of water inlet velocity, water inlet temperature, steam pressure and degree of steam superheating have been studied on the amplitude of pressure oscillations. The first and second dominant frequencies of pressure oscillations have also been obtained and studied. For most of the cases, the first dominant frequency peak was observed in the range ~ 0-1400 Hz whereas, the second dominant frequency peak was in the range ~ 2500 Hz - 3000 Hz. The first pressure peak was observed near the inlet of subcooled water such that its amplitude was increasing with increasing inlet water velocity but was nearly independent of inlet water temperature. Similarly, degree of steam superheating has no noticeable effects on pressure oscillations. It was observed that at a constant water temperature and water injecting velocity, the location of the pressure peaks was independent during the study. Further, the dominant frequency prediction map has been developed for the steam-water interaction in a pipe. The present study is assumed to be beneficial towards unfolds various important facts regarding steam-water interaction in the relevant industrial applications.

© Published at www.ijtf.org

1. Introduction

The steam and water are common working fluids in industrial sector. The steam condense when it directly interacts with water. This direct contact condensation (DCC)

[*]*Corresponding e-mail*: engquddus613@yahoo.com (Abdul Quddus)

Nomenclature

D	diameter of steam pipe, m		
d	diameter of the water pipe, m	Δt	Time step, s
d_b	bubble diameter, m	Δp	differential pressure , Pa (bar)
E	energy, J		
G	evaporation-condensation flux, kg/m^{2}s	*Greek symbols*	
g	gravitational acceleration, m/s^2	α	volume fraction
h_{fg}	latent heat, J/Kg	ρ	density, kg/m^3
K_{eff}	effective thermal conductivity, W/m^{2}K	β	molecular absorption accommodation coefficient
$\dot{m}_{lv}$	mass transfer rate resulting from evaporation, kg/m^{3}s	μ	Viscosity, Pa.s
$\dot{m}_{vl}$	mass transfer rate resulting from condensation, kg/m^{3}s	v	specific volume (m^3/kg)
P	pressure, kpa (Bar)	*Subscripts*	
R	universal gas constant, J/mol K.	k	kth phase
r	inverse of the relaxation time (1/s)	b	buble
S_h	volumetric heat source term, W/m^3	*	saturation condition
t	flow time, s	Abbreviations	
T	temperature, K (^{o}C)	*CFD*	computational fluid dynamics
v	velocity, m/s	*CIWH*	condensation induced water hammers
		NPPs	nuclear power plants
		LOCA	loss of coolant accident

between subcooled water and steam is an important thermo-hydraulic phenomenon which is experienced in numerous industries such as thermal power industry, chemical industry, renewable energy systems, food industry, and in nuclear industry [1-4]. DCC process has attained enormous consideration among the scholars being an efficient way of transferring mass and heat energy. Furthermore, there is a little requirement for driving potential of DCC process. The phenomenon of the steam-water DCC depends upon several thermal, mechanical and physical factors. The complex interplay among these factors finally drives the steam-water DCC phenomenon [1, 3, 5, 6].

The DCC events under certain conditions can originate rapid condensation leading to production of fast and violent pressure oscillations. The dynamics of such pressure oscillations peaks resulting from violent condensation is known as condensation induced water hammers (CIWH) [5, 7-9]. The fast pressure surges produced from CIWH are of great importance, specially, when pressure oscillations frequency become comparable with natural frequency of the relevant equipment. As a result the resonance phenomenon takes place which imparts extra load and may cause damage in the form of vibratory loads [10-13]. This vibratory load is harmful and could endanger the integrity of structures causing possible mechanical failure of piping, equipment and systems in many industrial applications. Therefore, it is important to know the underlying physics of pressure oscillations caused by DCC events.

Literature survey depicts that many scholars have explored the phenomena of pressure oscillations caused by steam-water DCC mainly including intensity, amplitude and dominant frequency etc. It was observed by Chan et al., [14] that pressure oscillations in typical condensation regime chugging and bubbling during vertical steam jet injection in

the quiescent pool of subcooled water was due to bubble collapse. Yuan et.al [10] conducted a study on the pressure oscillations in condensation oscillations (CO) region. They found that oscillations frequency decreased with increase in subcooled water temperature and steam mass velocity. The frequency of pressure oscillations during DCC with a horizontal steam jet at mass flux in the range of 300–900 kg /m^2 s was studied by Hong et al. [15]. CO and stable condensation (SC) regions were observed at steam mass flux greater than and less than 300 kg/m^2s, respectively. It was observed that the periodic oscillations of the steam plume causes creation of SC regime.

Aya in their work [16, 17], explored the dynamic pressure in chugging regime. They found that amplitude of pressure oscillations becomes stronger at low water temperature. It was found by Fukuda [18] that frequency in CO varies directly with water subcooling and inversely with the diameter of nozzle. Investigation on the steam jet pattern in SC region was made in study of Zhao [19]. It was pointed out that pressure peaks result from the combined effect of variation in length of steam cavity and bubble oscillation.The studies on the pressure oscillations by Qiu et al., [11, 20] for a horizontal steam jet in the SC regime showed that the first dominant frequency was primarily linked with the periodical oscillations of steam plume, whereas the second dominant frequency was mainly due to condensation and collapsing of the larger steam bubbles. The similar kind of results were reported in the work of Ref. [21]. The existence of the second dominant frequency in SC regime was also verified [8, 12].

Cho et al., [22] investigated the phenomenon of pressure oscillations with a horizontal steam jet condensation. They found that the pressure oscillations were stronger in CO regime then in SC region. The pressure oscillation frequency in the CO regime for horizontal jet was explored by Yuan et al., [10]. They also proposed an accurate thermal-hydraulic model to determine the main frequency of steam bubble oscillation. Few experimental studies by Wang et al.[23, 24] were performed to investigate steam-water CIWH and oscillations process under different operating conditions. Barna et al., [25] conducted an experimental and theoretical study on CIWH in a wide range of steam pressure. The pressure oscillations characteristics from condensation of vertical steam jet at low mass flux was studied by Yang [4].They indicated that the oscillation frequency for vertical steam jet was higher than for downward steam jet condensation.

There exist different industrial applications where subcooled water is injected into steam like steam de-superheated system [26] and in emergency core cooling spray system (ECCS) in nuclear power plants (NPPs) [1, 9, 27-29]. In NPP, injection of subcooled water into a steam-filled section is considered as an effective way for heat removal during accidental and transient situations to avoid core damage [9]. When loss of coolant accident (LOCA) occurs in pressurized water reactors (PWR), injection of subcooled water is made from the ECCS either into hot or the cold leg of the nuclear reactor [1]. Such kind of situations are also experienced very frequently in the feed water line of steam generator of PWR during operating and transient condition.

There is relatively limited experimental and computational data available on pressure oscillations induced by water injection into steam filled section. In experimental approaches, the precise synchronized results of many flow field information on pressure oscillations process are challenging to measure. Thus, the numerical simulations could provide more useful information about pressure oscillations. Most of the previous numerical simulations were focused on injection of steam in the test section [27, 30-32]. The numerical study of pressure oscillations mechanism in DCC with water injection is quite rare. Although the study of injecting subcooled water into steam filled section as in work [7, 25, 33-35] is capable of capturing the transient temperature history, heat transfer and flow regime transition resulting from interfacial instability. Summarizing the previous studies on pressure oscillations in steam-water DCC, researcher primarily focused on the

condensation occurring within quasi-static water pool. However, the present research in the confined spaces focuses mainly on water injection into steam filled test section instead of steam injection into subcooled water.

The purpose of this study was to investigate the characteristics of frequency and amplitude of pressure oscillations through CFD analysis. In this work, sub cooled water has been injected into a horizontal pipe filled with steam. The CFD methodology was validated by comparing the results with the published numerical results Datta et al.,2018 [33] as well as with experimental results of Barna et al.,2010[25]. After validation, the parametric effects of water inlet velocity, its temperature, steam pressure and steam superheating on the frequency and amplitude of pressure oscillations have been discussed in details. The study of dominant frequency from injection of water into steam has been conducted for the first time to the best of authors' knowledge and it is assumed that it will unfolds various important facts regarding steam-water interaction. A deep understanding related physics of pressure oscillations is considered to be beneficial towards the safe design and operation of steam based relevant industrial applications simulation, where time efficiency is important.

2. CFD simulations

2.1 Problem description and CFD models

In this numerical study, a water was injected into a stagnant steam present in a pipe has been studied computationally in two-dimensional domain, using commercial CFD software ANSYS Fluent. The geometry of the computational domain has been shown in Fig. 1. The initial and boundary conditions considered in the present study are also shown in Fig. 1. In this work, steam–water interaction phenomenon has been taken in a horizontal pipe with internal diameter as 66 mm and length of 2500 mm. The L/D ratio for the selected pipe is 37.87 ≈38). At the start of the simulation test section is assumed to be filled with dry saturated steam. Simulations are started as the subcooled water from 40 mm diameter pipe injected into test section. Beside adiabatic, the walls of the pipes are assumed with no-slip boundary conditions.

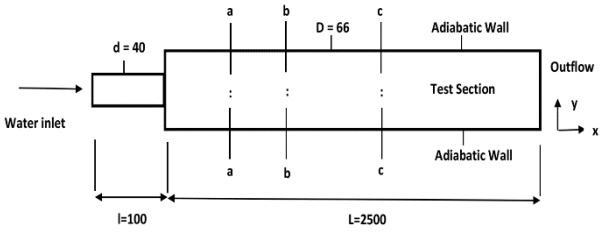

Fig. 1 Two-dimensional block diagram of the geometry with boundary conditions and physical dimensions (all dimensions are in mm)

The detailed operating conditions for this study work have been shown in Table 1, Table 2 and

Table 3 Velocity inlet boundary condition was taken to study the effects of water injecting velocity, its temperature and steam superheating while pressure inlet boundary conditions was taken for study of differential pressure effects (where differential pressure is the pressure difference between injecting water pressure and steam pressure). The standard thermo-physical properties for both steam and water phase are used. The steam-water condensation process was explored via 2D transient simulations.

The Volume of Fluid (VOF) model has been used to simulate the two-phase steam-water DCC problem. VOF method accurately predicts the interface and has superior volume conservation as compared to any other volume tracking methodology or fixed grid interface approaches [27, 33, 36-38]. The turbulence nature of flow was captured by using realizable k-ε model. Previous studies [33] showed that result of k-ε model are equal good for flow in a restricted channel geometry [7, 33, 39]. Realizable k-ε turbulent model further addresses the weakness of the standard k-ε model [30, 38, 40]. Time discretization for the transient analysis was based on the basis of implicit scheme. The famous SIMPLE algorithm scheme was adopted for pressure–velocity coupling. Discretization of continuity equation was made by PRESTO scheme [41].

The solution methods for momentum, volume fraction, energy, turbulent kinetic energy and dissipation rate equation are based

on second order upwind method. The simulations have been performed for a real time of 2 second with fixed time step of 100 micro-sec. Thus time duration was enough that for even smallest water velocity (i.e.1m/s), effect from wave front of subcooled water was reached at the outlet of the geometry well before the duration of 2seconds (as shown in Fig. 8(a)). Form the previous DCC studies, it could also be seen that total time duration for studying pressure oscillations was kept even less than 2seconds i.e 100 ms [42], 1.8s [43], 0.5s[44], 0.21s[45]. The single time step is set small enough so that criteria for the Courant number remains less than one during the simulations is met [46].The detailed work on time step independence is shown the coming grid independence section. All the residual limits for convergence criteria are set below $1.0x10^{-3}$ except for energy residual which is set below$1.0x10^{-6}$. The present study also considered the assumption of both steam and water as incompressible phases. This assumption works good when operating pressure is above 10 kPa [27]. Further the results in the work Datta et al. [33] Quddus et al.,[47] and Shukla et al., [27] strengthen this assumption. The frictional effects of the pipe were ignored which have negligible effects on pressure oscillations as seen in the Ref. [5, 47, 48]. The Lee mode assumes constant saturated temperature within the bulk vapour phase and at steam-water interface which has been taken as model default value as 100^{o}C [48, 49]. If the temperature of the computational cell differ from saturated state then mass transfer is calculated from local superheating or super cooling [49] as described in section 2.2.5.

Table 1
Operating conditions for variation in injecting velocity

Water Injection Velocity (m/s)	Water Temperature (^{o}C)	Steam Pressure (kPa)	Steam Temperature (^{o}C)
1, 3, 5 and 7	20	600	158.80
	30		
	40		
	50		
	60		

Table 2
Operating conditions for steam-water differential pressure variation

Water Pressure (kPa)	Water Temperature (^{o}C)	Steam-Water ΔP (kPa)	Steam Temperature (^{o}C)
1200	40	800	143.61
		600	158.80
		400	170.40
		200	179.88

Table 3
Operating conditions for variation in steam superheating effects

Water velocity (m/s)	Water Temperature (^{o}C)	Steam Pressure (kPa)	Steam Degree of superheating (^{o}C)
5	40	600	2
			6
			8

2.2 Governing Equations

In the present study, VOF approach has been used for modelling the steam–water DCC process. The VOF model can track the volume fraction of each phase throughout the fluid domain. VOF method accurately predicts the interface and has superior volume conservation as compared to any other volume tracking methodology or fixed grid interface approaches [27, 33, 36, 38]. The basic governing equations which speaks the basic DCC process are mass conservation, momentum conservation, energy conservation, turbulence, heat and mass transfer coefficients at interface and the condensation and evaporation model [38]. Brief details of these equations are presented as below;

2.2.1 Mass conservation equation:

Continuity equation for any phase 'k' can be written as:

$$\left[\frac{\partial(\alpha_k\rho_k)}{\partial t}+\nabla.\left(\alpha_k\rho_k v\right)\right]=\dot{m}_k \tag{1}$$

Where, α, ρ and v are volume fraction, density and velocity of the phase 'k', respectively. The volume fraction is calculated keeping in view the following constraint.

$$\sum_{k=1}^{n}\alpha_k=1 \tag{2}$$

2.2.2 Momentum equation

A single momentum equation is solved throughout the fluid domain. The resulting velocity field obtained from momentum equation is shared among all the phases. The momentum equation depends upon the volume fraction, density and viscosity of all phases. The momentum equation is shown as;

$$\frac{\partial(\rho v)}{\partial t}+\nabla.\left(\rho vv\right)=-\nabla.\mathrm{p}+\nabla.\left[(\mu(\nabla v+\nabla v^{T})\right]+\rho g+F \tag{3}$$

Where, p, g, F and μ are pressure, gravitational acceleration, body force present and viscosity of the fluid respectively.

2.2.3 Energy equation

The energy equation shared among the phases is;

$$\frac{\partial(\rho E)}{\partial t}+\nabla.\left(v(\rho E+p)\right)=\nabla.\left(K_{eff}\nabla\,\mathrm{T}\right)+S_h \tag{4}$$

$$E=\frac{\sum_{k=1}^{n}\alpha_k\rho_kE_k}{\sum_{k=1}^{n}\alpha_k\rho_k} \tag{5}$$

Where E, keff and T are energy, effective thermal conductivity and temperature respectively. The energy for individual phase Ek is dependent on the shared temperature and its specific heat. The volumetric heat source term S_h, is consistent with the mass transportation at the interface and is computed by product of latent heat with rate of mass transfer.

2.2.4 Realizable k-ε model

The Realizable k-ε model for each phase is selected to capture turbulence phenomenon in the present system. The modelled transport equations for turbulence kinetic energy (k) and its dissipation rate (ε) model are;

$$\frac{\partial(\rho k)}{\partial t}+\frac{\partial(\rho ku_j)}{\partial x_j}=\frac{\partial}{\partial x_j}\left[\left(\mu+\frac{\mu_t}{\sigma_k}\right)\frac{\partial k}{\partial x_j}\right]+G_k+G_b-\rho\varepsilon-Y_M+S_k \tag{6}$$

$$\frac{\partial(\rho\varepsilon)}{\partial t}+\frac{\partial(\rho\varepsilon u_j)}{\partial x_j}=\frac{\partial}{\partial x_j}\left[\left(\mu+\frac{\mu_t}{\sigma_\varepsilon}\right)\frac{\partial\varepsilon}{\partial x_j}\right]+\rho C_1S\varepsilon-\rho C_2\frac{\varepsilon^2}{k+\sqrt{v\varepsilon}}+C_{1\varepsilon}\frac{\varepsilon}{k}C_{3\varepsilon}G_b+S_\varepsilon \tag{7}$$

Where Gk and Gb denotes the generation of turbulence kinetic energy due to the mean velocity gradients and buoyancy respectively. YM represents the contribution of the fluctuating dilatation in compressible turbulence to the overall dissipation rate. C1Ɛ= 1.44, C2Ɛ =1.92, σ_k =1.0 and σ_ε = 1.3.

2.2.5 Evaporation-Condensation model

Selection of condensation model plays a

critical role in the numerical study of pressure oscillation during steam-water DCC. Some previously developed models like RELAP5 and CATHARE were unable to predict pressure peaks generated from CIWH [25, 50, 51]. In present study, Lee model in combination with Evaporation-condensation model [27,52] has been selected. This condensation model and ANSYS FLUENT can predict the DCC phenomenon and pressure oscillations [27, 33].

The Lee evaporation-condensation model [52] is a mechanistic model with a physical basis [38]. The transportation of mass from steam-water is primarily governed by following vapor transport equation:

$$\frac{\partial(\alpha_k \rho_k)}{\partial t} + \nabla.(\alpha_v \rho_v v_v) = \dot{m}_{lv} - \dot{m}_{vl} \quad (8)$$

Where αv , vv and ρv are vapor phase volume fraction, steam phase velocity and density respectively. While $\dot{m}_{lv}$ and $\dot{m}_{vl}$ are the mass transfer rate resulting from evaporation and condensation (in kg/m3sec) respectively.

When the temperature of interfacial cell is different from the saturation temperature then the Lee model [52] consider the mass transfer on the basis of the temperature regimes as;

If Tl> T sat (evaporation):

$$\dot{m}_{lv} = coef.f * \alpha_l \rho_l \frac{(T_l - T_{sat})}{T_{sat}} \quad (9)$$

If Tl< T sat (Condensation):

$$\dot{m}_{vl} = coef.f * \alpha_v \rho_v \frac{(T_{sat} - T_l)}{T_{sat}} \quad (10)$$

In the present study the temperature of the water phase lies in the range of 20-60°C which is less than the saturated temperature of the steam (143.6-179.9 ℃) as shown in Table 1 and Table 2. The mass transfer would rely through condensation phenomenon.

The coefficient coef .f, ρ and α are relaxation time, density and phase volume fraction respectively.

The evaporation-condensation flux (kg/s/m2) based on the kinetic theory is computed by Hertz Knudsen formula;

$$F = \beta\sqrt{\frac{M}{2\pi R T_{sat}}}\left(P^* - P_{sat}\right) \quad (11)$$

Where accommodation coefficient, β, is the portion of vapor molecules being adsorbed by the liquid surface. T is the temperature, P is the pressure, R is the universal gas constant and P^* represents the interface vapor partial pressure on the vapor side.

The Clapeyron-Clausius equation is used to relate pressure with temperature at saturation condition;

$$\frac{dP}{dT} = \frac{L}{T(v_v - v_l)} \quad (12)$$

Where v_v , v_l are the specific volume of the vapor and liquid respectively and L, represents the latent heat when P* and T* approached the saturation condition:

$$\left(P^* - P_{sat}\right) = \frac{L}{T(v_v - v_l)}\left(T^* - T_{sat}\right) \quad (13)$$

$$F = \beta\sqrt{\frac{M}{2\pi R T_{sat}}} L\left(\frac{\rho v \rho l}{\rho l - \rho v}\right)\frac{\left(T^* - Tsat\right)}{Tsat} \quad (14)$$

By assuming all vapor bubbles is of uniform diameter, then the interfacial area density in term of bubble diameter d_b, is computed by the following mathematical expression:

$$Ai = \frac{6\alpha_v \alpha_l}{d_b} \quad (15)$$

Then the phase source term (kg/s/m^3) attains the following form:

$$FAi = \frac{6}{d_b}\beta\sqrt{\frac{M}{2\pi R T_{sat}}} L\left(\frac{\alpha_v \rho_v}{\rho l - \rho v}\right)\left(\alpha_l \rho_l \frac{\left(T^* - T_{sat}\right)}{T_{sat}}\right) \quad (16)$$

From the above expression Coef .f which is inverse of the relaxation time (1/s) can be defined as;

$$coef.f = \frac{6}{d_b}\beta\sqrt{\frac{M}{2\pi RTsat}}L\left(\frac{\alpha_v\rho_v}{\rho l-\rho v}\right) \quad (17)$$

2.2.6 Pressure oscillations

The pressure rise due to condensation induced water hammering transients defines the dynamic pressure changes during condensation. This increase in pressure amplitudes results from condensation of an entrapped pocket of saturated steam which is surrounded by subcooled water. For a single CIWH event, the change in pressure can be described by Joukowsky's equation. However, previous studies showed that the results from Joukowsky's equation were either unrealistically underestimated or dangerously overestimated. This equation calculated the CIWH intensity for vertical pipe and large errors were predicted in pressure peak results for horizontal flow pipe. [9, 29]. Furthermore this equation assumes that fluid properties remains constant. This assumption is not applicable for our case (two-phase transient flow) where temperature does not remains homogeneous. Therefore, the pressure in the present study pressure calculations were from ANSYS Fluent built-in equations. The related mathematical details on pressure calculation can be seen in the theory manual of ANSYS Fluent [38].

2.3 Grid independence

Grid independence study is carried out to obtain an appropriate grid size on which the solution of the given problem become independent of the grid size. The grid independence study for the present case has been executed by plotting liquid volume fraction variation at a vertical line 400 mm (section a-a in Fig. 1) from the inlet of water. The same simulations were repeated by using five different cell sizes with same models and settings. The cell sizes used are Δx =0.75, 0.90, 1.15, 1.5, and 2 mm. The liquid volume fraction distributions, at a vertical line 400 mm from the water inlet, using five different cell sizes have been shown in Fig. 2. From this Fig. 2, it can be seen that behaviour of volume fraction variation distribution at grid sizes of $\Delta x = 2$ mm and 1.5 mm is not consistent with the distribution profiles for the rest of the grid size cases. For grid size 2 mm, there is late start in the rising of water volume fraction curve while at grid size 1.5 mm, the curve fluctuates more violently. The solution is not trust worthy unless it became independent of grid size. Therefore, solution for these two grid sizes does not reflect the true behaviour of the condensation phenomenon and is grid dependent. But when the element size is reduced to 1.15 mm, the volume fraction distribution at the indicated location becomes independent of the grid size. Therefore, $\Delta x = 1.15$ mm (corresponds to 108640 number of computational cells) has been selected and used for numerical simulations of the present work. The volume fraction values clearly exhibit a similar trend, i.e., the liquid volume fraction initially is zero as liquid phase in absent in the test section at the start of the simulation. It increases and finally reaches to unity indicating the onset of local flooding condition at the particular location. Thus, a cell number of 108640 corresponding to cell size $\Delta x = 1.15$ mm is adopted in the present simulation work to ensure accuracy of the solution and to save computational time.

The time step independence analysis for the current work has been carried out in term of temperature values at the axial location of 0.4m from the water inlet (section a-a in Fig. 1) within the test section. This study is repeated at three different time, $\Delta t = 10^{-3}$, 10^{-4} and 10^{-5} with a specific cell size Δx =1.15mm. For each case, the inlet velocity of the injected subcooled is kept at 5m/s at temperature 293.15K. Fig. 3 shows that the change in the calculated temperature values is the negligible when Δt changes from 10^{-4} to 10^{-5}. Therefore, $\Delta t = 10^{-4}$ is selected for further simulations. The simulations have been performed for a real time of 2 seconds with fixed time step of 100 micro-sec. The time step size was also verified on best approach of minimum grid size and highest velocity by using the relationship between Courant-Friedrich-Levy number, velocity v, time step Δt , and grid spacing Δx , $\left(CFL = \frac{v.\Delta t}{\Delta x} \le 1\right)$ [46].

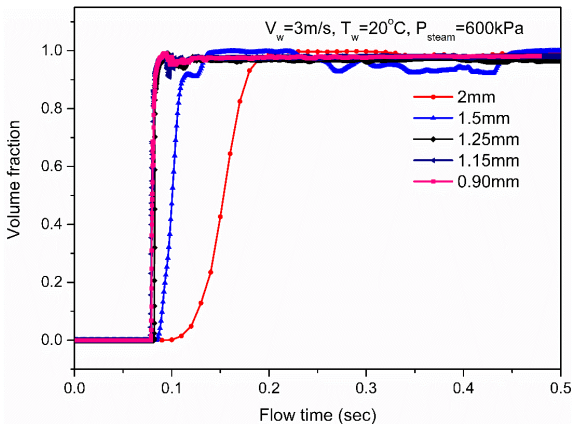

Fig. 2. Mesh independence study in terms of volume fraction variation at 400 mm from the beginning of the test section for water injecting velocity of 3 m/ s.

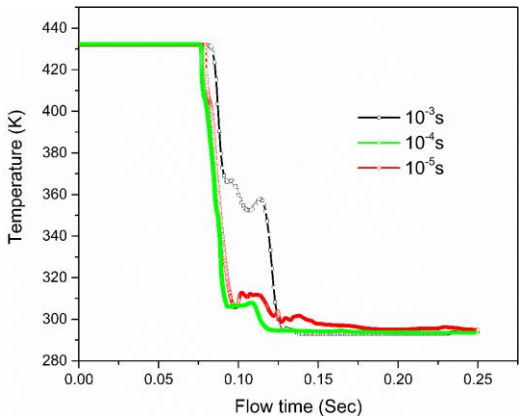

Fig. 3. Temperature history for different time steps at axial location at 400 mm from the beginning of the test section for water velocity of 5m/s, $\Delta x = 1.15$ mm and inlet water temperature of 20°C (293.15K).

2.4 Validation of CFD methodology

In order to check the correctness and validity of the CFD methodology, it is important to compare the simulation results with the experimental or reported results in the literature. The only published results available for water injection into steam pipe for the given geometry are those of Datta et al. [33]. Therefore, the results of Datta et al. [33] and Barna et al. [25] have been used for validation of the CFD methodology in this study. Furthermore, since the current study is mainly focused on pressure oscillations, therefore, Barna's experimental work on pressure oscillations [25] was also used to verify the simulations results.

The effect of water inflow at velocity 5m/s on the radial temperature distribution as well as on the interface behavior at location of 800 mm (section b-b in Fig. 1) and 1400 mm (section c-c in Fig. 1) from inlet is studied. The water temperature was maintained at 293.15K. Thus simulation for average radial temperature distribution for water velocity of 5m/sec within the test section at said location was compared with the results of Datta et al. [33] as shown in Fig. ***4***. It has been found that the temperature of the mixture initially remained constant prior to arrival of the liquid phase at the indicated location. As soon as the condition of local flooding is arrived, temperature suddenly decreased. Furthermore, the contour of the liquid volume fraction obtained at flow time of 1.2 sec with water velocity of 1 m/s and 5 m/s. Volume fraction of water captured in present work was compared with the results of Datta et al. [33]. These results have been shown in Fig. 5.The comparison of results indicated that the temperature and liquid volume fraction were identical with the earlier study of Datta et.al [33]. In Fig. ***4***(a,b),comparison of present results with findings of Datta et.al,2018 [33] shows that for temperature profile, the data before and after the fall in curves lies within maximum error of 12.3% and 20% with time shift of 4ms and 6.8ms at location 0.8m and 1.4m from inlet, respectively.

Since the present work is related with pressure oscillations, therefore the results were also validated with experimental work on pressure oscillations by Barna et.al, 2010[25]. where horizontal pipe having diameter 0.073m, length 3m ,initially filled with steam at 14.5 bar (1450 kPa) at temperature 470 K) was simulated with subcooled water injection at velocity 0.242m/s and temperature 22°C(295.15 K). The pressure transients history were measured at 0.4m from left elbow which was much consistent with the experiments by Barna et.al, [25] as shown in Fig. 6. The value of the pressure peak is about same order (i.e. 165 bar (16500kPa) in our case against 174 bar (17400kPa) in experimental work of Barna et al., 2010) but with little time lag. The maximum amplitude

of the pressure is more important than its time to occur. For pressure oscillation, the comparison of present study with the experimental work of Barna et al.,[25] shows maximum error of 5.45% exists in the results. However, there is time shift of 2.4ms between the peak curves. Thus, it is concluded that the simulation results are quantitatively and qualitatively consistent with the outcome shown in [25, 33] , suggesting the validity of the selected CFD methodology.

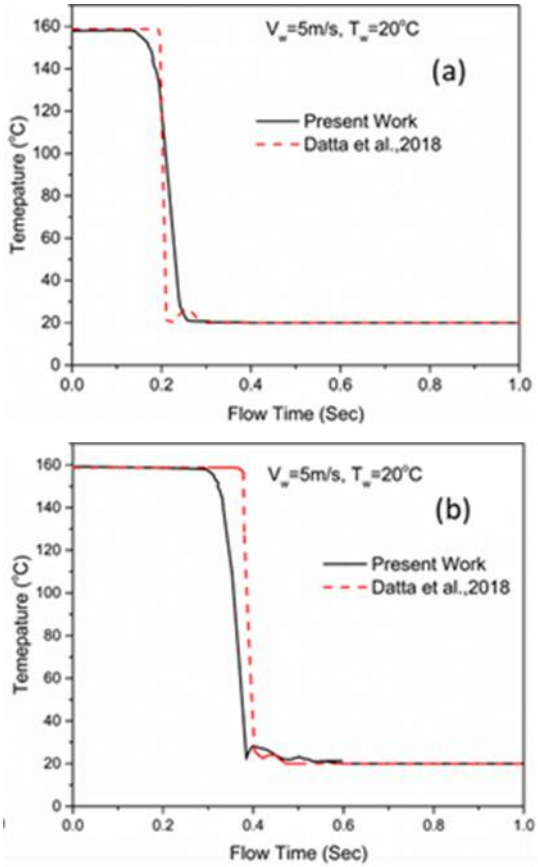

Fig. 4. Variation of test section temperature with flow time at water injection velocity 5m/s at location (a) 0.8 m (b) 1.4 m from the beginning of the test section.

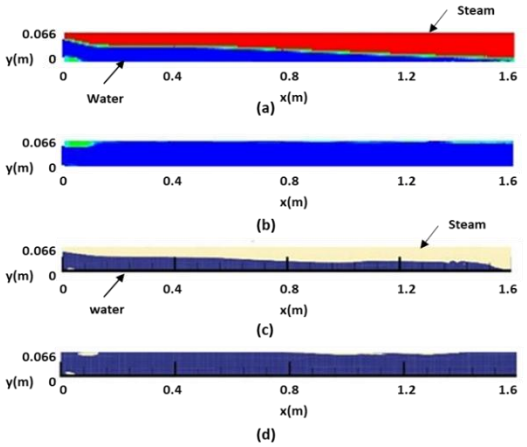

Fig. 5. Comparison of contour of water volume fraction between present study (a, b) and Datta et al., 2018 work (c, d) [33] computed at flow time of 1.2 sec for water velocity 1m/s (a, c) and at 5m/s (b, d)

Since the present work was validated with Datta et al.,2018[33] whose work was successfully validated both numerically and experimentally. Therefore results of present 2D study can be reliable. Moreover, some previous researches have also shown that a 2D simulation can reliably predict the DCC phenomenon in a pipe [33, 36, 37]. Furthermore, 2D models can predict the instability and transformation of the stratified flow into the slug flow [7]. Similarly in present study, steam was assumed to be as incompressible phase. This assumption works good when operating pressure is above 10 kPa [27]. Further the results in the work Datta et al. [33] and Shukla et al., [27] strengthen this assumption.

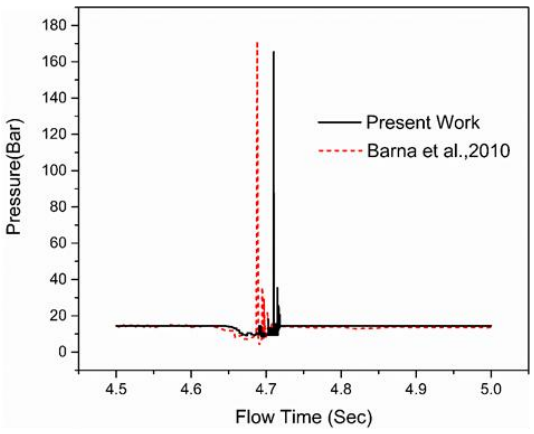

Fig. 6. Comparison of transient pressure history with the published work of Barna et al. [25].

4. Results and discussion

In this work, CFD study on pressure oscillations induced by water injection into steam filled section in a horizontal pipe has been performed. The DCC of steam injection into subcooled water has been investigated by many scholars [27,30-32]. However, the injection of subcooled water into a steam filled test section has not been studied in depth so far and is the main topic of the present study.

The numerical study of injection of subcooled water into steam filled section as in the previous published work [7, 33-35] is capable of capturing the transient temperature history, heat transfer and flow regime transition resulting from interfacial instability. However, it may be equally useful for studying the pressure oscillations with their dominant frequencies, which has been considered in the current study. Fast Fourier transformation (FFT) has been used to obtain the first and second dominant frequencies. These pressure oscillations frequencies become important when fall close to the natural frequency of the relevant equipment. As stated earlier, the resonance phenomenon may take place which imparts additional load. It could endanger the integrity of the equipment and systems in many industries especially in nuclear industry [7, 9, 30, 53], where a single accident is not affordable due to radioactive release.

In this section the parametric effects of water inlet velocity, water temperature, steam pressure and steam superheating effects on the frequencies and amplitude of pressure oscillations have been studied and discussed in details. The results have been validated with the work in Ref. [33] and [25].

4.1 Effect of water injecting velocity on pressure oscillations

This section presents the parametric effect of variation of water injecting velocity on the pressure oscillations during steam–water interaction. The water has been injected at constant temperature of 40^{o}C into a steam filled test section at pressure of 600 kPa and temperature of 158.8 ℃. The subcooled water injecting velocity has been varied as 1, 3, 5 and 7 m/sec. Fig. 7(a-d) shows the variation of pressure with time at section a-a within the steam pipe for 2 seconds time span at above said water inlet velocities. Pressure peaks having different magnitudes i.e. around 624, 672, 720 and 768 kPa have been observed against water injecting velocity of 1, 3, 5 and 7 m/s respectively. It has been observed that a strong pressure pulse is generated in a short time near the injecting point, as the subcooled water enters into the test section. The dynamics of such pressure pulses under the influence of violent condensation is due to CIWH phenomenon, which results in fast pressure surges [5, 9].

From Fig. 7(a-d), it can be clearly seen that with the increase in injecting water velocity, there is an early start of pressure oscillations. This is due to fact that as water velocity is increased, the water wave front moves more rapidly into test section which condense the steam within shorter time. As stated earlier, this violent condensation of entrapped steam pockets causes the onset of pressure oscillations. Especially when velocity is increased from Vw =1 to 3, m/s, pressure oscillations starts around ~0.7s. With further increase in water velocity Vw =5m/s, the more pronounced pressure oscillations persist due to the creation and collapsing of more steam pockets. However, at water velocity Vw =7m/s, the intensity of pressure fluctuation suddenly decreases at ~1.3s as shown in Fig. 7 (d). This decrease is due the reason that at higher water velocity water wave front penetrated deeper into steam section. Resultantly, large portion of steam condensed in a shorter time. After condensation of larger volume of the steam, less quantity of the steam would left behind in the test section. Smaller the steam quantity present within the test section, less steam pockets would be formed. As a result the pressure oscillations decreases

From Fig. 7 (a-d), it is revealed the weak pressure oscillations are observed at smaller injecting velocity but strong oscillations have been noticed at higher velocities. This difference in behaviour is due to the fact that for smaller injecting velocity, V_w =1m/s,

momentum imparted by water inflow is smaller which established stratified flow regime (steam vapor phase located at top while water on bottom, shown in Fig. 8(a). When subcooled water is injected with larger velocities into steam filled pipe, the water wave front moves into test section. This movement of wave front make the interface as wavy. When it touches the pipe wall, onset of bridging phenomenon takes place as shown in Fig. 8(b). This figure shows the qualitative distribution of volume faction along the length of pipe.

Fig. 8(c,d) describe the movement of water wave font at flow time of 0.1s. When this wave front moves into steam section, it encapsulate the steam pockets [54] which can be seen in Fig. 8(c,d). The rapid condensation of this entrapped steam causes localized low pressure zone. The pressure difference between this condensation region and surrounding liquid phase accelerates the subcooled water towards lower pressure region. Higher the velocity, more inertial force will be there. This inertial force come from accelerated water wave front which compresses the low pressure area [23]. This compressive action and collision of water molecules during rushing rises the pressure in the region which appeared in the farm of first instantaneous pressure peaks as shown in Fig. 7 (a-d).With the passage of flow time, the large portion of steam within the test section is condensed. Resultantly, the pressure oscillations decreases. The decrease in pressure oscillations strength is rapidly observed for higher injecting velocity case as shown in Fig. 7 (d) where steam condensed within the test section in shorter time.

When bridging phenomenon occurs, the transition from stratified flow to slug flow regime took place for water injection velocity of 3 m/s, and 5 m/s. This transition of flow regime was the basic driving regime for pressure oscillations. The pressure pulses generated by higher injected water velocities became more vigorous and larger in magnitude than the pressure pulses generated by lower injected water velocities. Whereas, Fig. 9 shows the variation in volume fractional of water at three different locations within the pipe i.e. 0.4m,0.8m and 1.4m away from inlet. The fluctuations in volume fraction in this plot further confirm presence of steam pockets and bridging within the pipe.

The variation of first instantaneously generated pressure peak at different velocities at section a-a within the steam pipe has been shown in Fig. 7 (e). The straight line in this figure indicates that at a constant velocity value, the first instantaneously generated pressure peak near the water injecting point is independent of subcooled water temperature. From Fig. 7 (e), it is also concluded that the value of this peak increases with injected velocity at a constant temperature. It has also been observed that with the increase in water injecting velocity, the transition from stratified to slug is shifted upstream causing pressure oscillations to start earlier with higher values in pressure magnitude due to above stated reason. Another reason for variation in pressure oscillations was due to growth, propagation, and detachment of the interfacial wave developed during DCC phenomenon. This disturbance in the steam-water interface grows due to the mechanism of Kelvin–Helmholtz instability [5, 55-57].

4.2 Effect of injecting water temperature on first instantaneous pressure peak

In this section, effect from temperature of injected subcooled water on first instantaneous pressure peak generated near the water inlet within the test section, has been considered. These simulations have been carried out at five different inflow water temperatures 20, 30, 40, 50 and 60 ℃ for four different water velocity of 1, 3, 5 and 7 m/s repeatedly as again shown in Fig. 7 (e). It is observed from Fig. 7 (e) that for a fixed value of velocity, straight lines show the value of first instantaneous pressure peak generated is independent of temperature within the mentioned temperature range 20-60^{o}C. It became obvious that the pressure oscillations caused by onset of water flooding at the starting location of test section is mainly dependent on the velocity values of the injected subcooled water instead of its temperature. Thus, imparted momentum of the

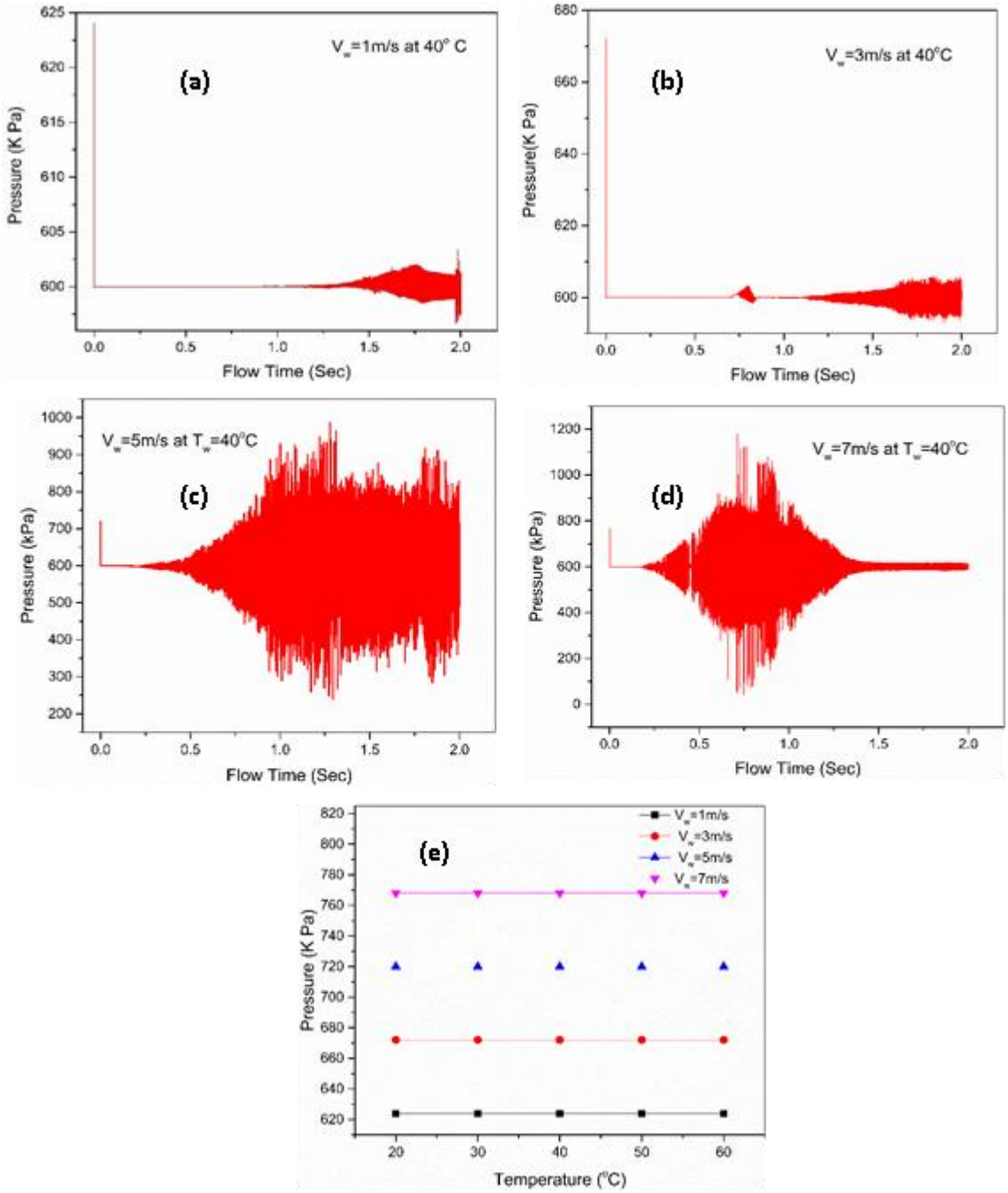

Fig. 7 Variation of pressure with time in the test section at different water injection velocity (a) 1m/s (b) 3m/s (c) 5 m/s (d) 7m/s (e) Variation of first instantaneous pressure peak with temperature at different water velocity

injected water into steam filled test section plays a vital role in pressure oscillations.

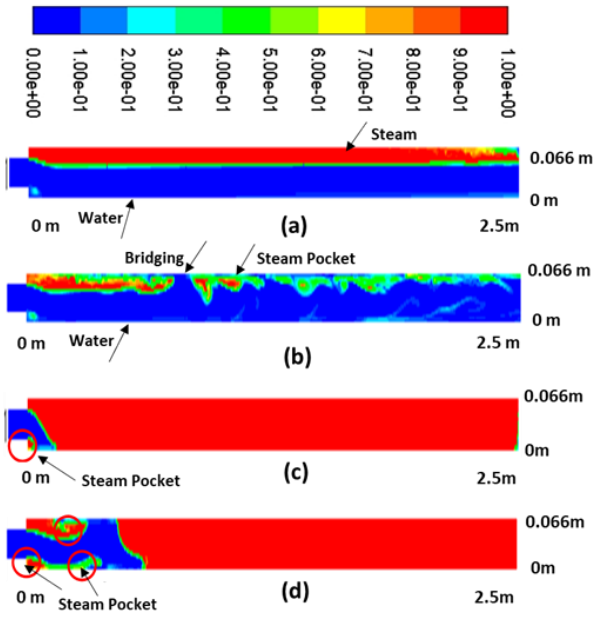

Fig. 8 Variation of water volume fraction along the length of the pipe **(a)** at water velocity 1m/s and temperature 40°C (stratified flow) **(b)** at water velocity 5m/s and temperature 40°C (slug flow) **(c)** at water velocity 1m/s and temperature 40°C and flow time 0.1sec **(d)** at water velocity 5m/s and temperature 40°C and flow time 0.1sec

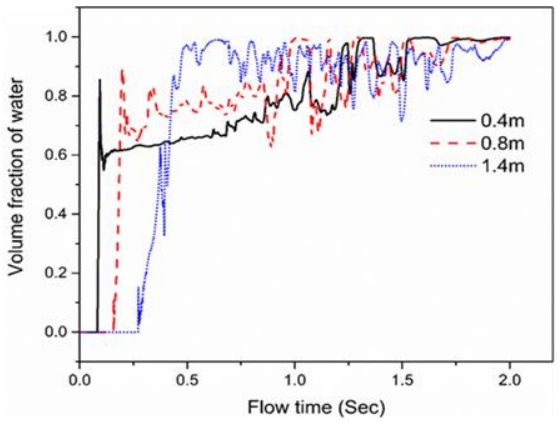

Fig. 9 Variation of water volume fraction with flow time at 5m/s and temperature 40°C at location 0.4m, 0.8m and 1.4m away from water inlet

4.3 Effect of steam pressure on pressure oscillations

Apart from temperature and velocity effect of injected subcooled water, the steam pressure also has a dominant role on pressure oscillations characteristics. In this section, pressure oscillations parameters have been investigated at different values of steam pressures i.e. 400, 600, 800 and 1000 kPa within the test section against a constant injecting water pressure of 1200 kPa and temperature, 40°C. These steam pressure corresponds to different steam-water differential pressure within the test section i.e. ΔP = 800, 600, 400 and 200 kPa respectively. The obtained results have been shown in the Fig. 10(a-d). The numerical range of the values at vertical axis of the each part of the Fig. 10, are kept different from each other to highlight the behaviour of oscillations. From Fig. 10(a-d), it could be revealed that when steam-water differential pressure in the test section was high, then increase in peak pressure and decrease in valley pressure has been observed in the pressure curves. This effect can be clearly observed at steam pressure 400 kPa (ΔP = 800 kPa) as shown in Fig. 10(a). When steam pressure in the test section is increased to 600 kPa and 800 kPa, then steam-water differential pressure in the test section reduces to 600 and 400 kPa, respectively. The pressure oscillations during steam condensation becomes weaker which are shown in Fig. 10(b-c). Similarly, at steam pressure 1000 kPa (ΔP = 200 kPa), results indicates that strength of the expansion and compression waves become further weakens as in shown in Fig. 10(d). This decrease in pressure oscillations might be due the decay in Kelvin-Helmholtz instability [5, 47, 48, 55-57].

The increase in pressure is again attributed towards condensation of entrapped steam pocket within the surrounding liquid phase as shown in Fig. 8(b-c). The increases in pressure is followed by drop in pressure from expansion-contraction theory. As the drop in pressure continues alternatively during series of expansion-contraction waves and from the decay in Kelvin-Helmholtz instability, the amplitude of the pressure oscillations becomes weaker [5, 47, 48, 55-57].

On the other hand, stronger expansion waves have been resulted when difference between steam pressure within the test section and injected water pressure widens. When

steam pressure drops due to condensation, expansion occurred. The area with low pressure zone is filled up by rushing of surrounding fluid making compression wave afterward. Thus, the strength of compression and expansion waves grew with decrease in steam pressure.

However, it is again noteworthy that as steam pressure is increased from 400 to 1000 kPa, expansion and compression waves comes closer to each other. This might be again associated with the fact that as steam pressure is increases then tendency to form steam pockets will increase. The condensation of these pockets is reasonable for pressure oscillations.

4.4 Effect of steam superheating on pressure oscillations

This section discuss the effect of steam superheating on the pressure oscillations. For this case study, water injecting velocity is kept constant at 5m/s and temperature 40^{o} C. Dry superheated steam is supposed to be initially filled at 600 kPa in the test section at the beginning of the simulations. The degree of steam superheating has been varied from 2oC, 6oC, and 8oC. Fig. 11 shows the pressure oscillations for different steam superheating at section a-a of the geometry shown in Fig. 1. From these Figures, it can be concluded that pressure oscillations are almost independent from effects of the steam superheating and does not affect the type of pressure oscillations. Similar kind of effects of steam superheating on DCC were found in the study of Celeta et al., [58]. Only minor variations exist in pressure oscillations with the change in degree of steam superheating. These negligible deviations may arise from the variation in local temperatures and pressure conditions for various degree of steam superheating.

Summarizing the results from Fig. 6, Fig. 7,Fig. 10 and Fig. 11, shows that variation in the pressure oscillations exist. It is complexity of the problem due to which variation in the nature of oscillation exists. For different operating conditions, the pressure fluctuation signals may either be continuous type or pulse type which can be seen in the work of Wang et al., 2020 [23, 24, 43, 59]. Numerous independent pressure peaks can appear during CIWH events [25, 60]. The pressure in the case shown in Fig. 6 is much higher than rest of the above cases as the amplitude of pressure peaks may vary in irregular manner with the change in system pressure [61] and their intensity is influenced by the condensation behavior of steam [9]. Most scholars concluded that it is highly stochastic and the prediction for CIWH events is strongly dependent on the initial and boundary conditions [9, 51] .

Similarly, the nature of pressure oscillations in the present study is different from the work of Datta, Chakravarty et al. 2018, who simulated the similar shape of the geometry. The other reason for this difference might be due to selection of different condensation models. In the present study Lee evaporation-condensation model was used while Datta, Chakravarty et al. 2018 used in-house 1D compressible code. This 1D model is based on different closure models. These authors stated that the prediction for CIWH events is strongly dependent on the closure models, initial and boundary conditions. Even the amplitude of the pressure peaks and their occurrence computed from different models may be different which can been seen in Datta et al.2018 work [33]. The other reason for deviation of the present result from Datta's findings [33] may be due to different inlet conditions and dissimilar water inlet diameter (i.e. the diameter of the inlet section in our case is 40 mm against 66mm inlet in Datta et al. work [33]). Such kind of variation in results at similar steam pressure but different diameter of the pipe geometry can even be seen by comparing Datta et al.2018 work with their another work [5].

4.5 Frequency spectrum analysis

Frequency spectrum in DCC is used to represent dynamic characteristics including amplitude and oscillations frequency of steam

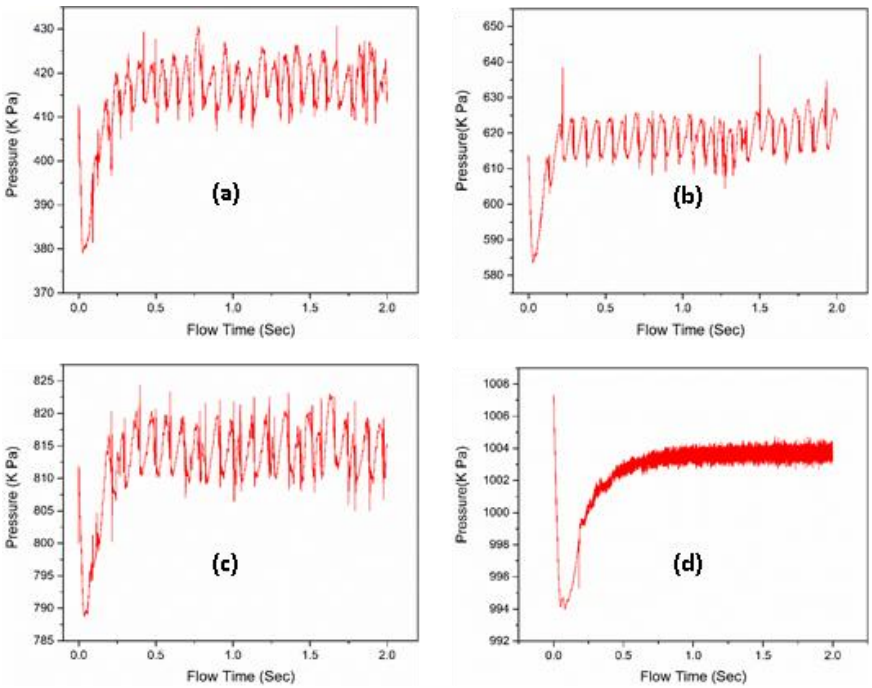

Fig. 10. Variation of pressure with time with water injected at 1200 kPa & 40^{o}C in the test section for different steam pressure (a) 400 kPa (b) 600 kPa (c) 800 kPa (d) 1000 kPa

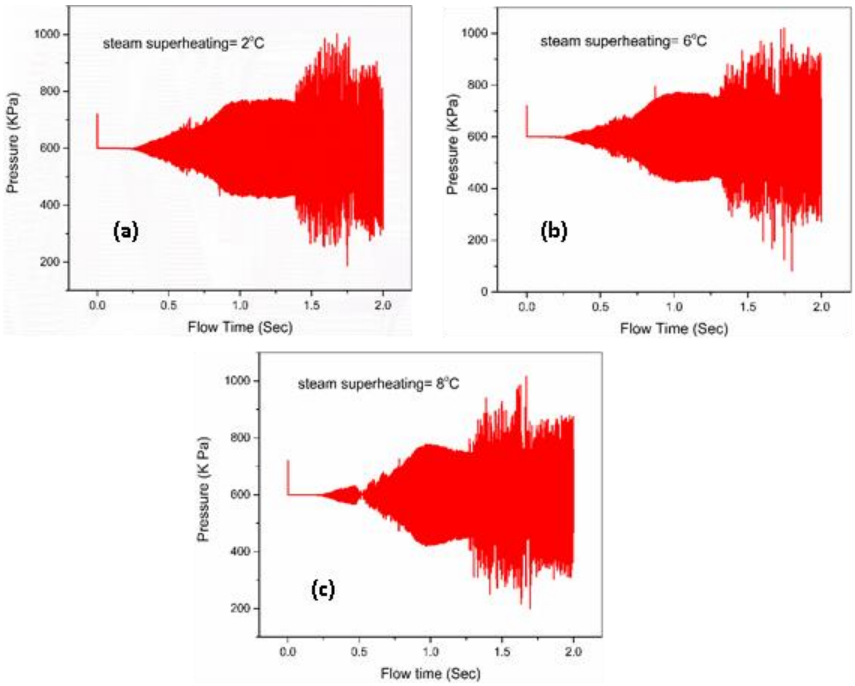

Fig. 11. Variation of pressure with time in the test section at different degree of steam superheating (a) 2^{o} C (b) 6^{o} C (c) 8^{o} C.

condensation in a narrow pipe. It is a complicated process and has strong randomness[62]. It becomes very hard to directly analyze pressure oscillations characteristics by using a time domain. Therefore, the FFT technique has been used to obtain the spectrum of pressure oscillations.

When subcooled water is injected into steam filled section of a pipe, various patterns of pressure oscillations may appear depending upon the balance of the energy shared between the liquid and vapor phases [9]. During this mixing, growth of interface wave taken place which is propagated downstream and finally detached. The pressure oscillations resulting from the interfacial wave disturbance with certain dominant frequency and amplitude takes place [63]. In the previous literature, researchers mainly focused on the first dominant frequency being lowest dominant frequency. As the natural frequency of fluid domain is also low, there is stronger possibility that oscillations may resonates. Besides first dominant frequency, the second dominant frequency peak only develops in certain transient conditions. Both the dominant frequency peaks have their own characteristics [12, 19, 42, 64].

Fig. 12 and Fig. 13 show the frequency spectrums of pressure oscillations for different steam pressure. In Fig. 12, pressure oscillations has been computed when water at 40 ℃ (313.15K) and 1200 kPa is injected into steam section at 600 kPa. Observations for pressure oscillations have been recorded at three different locations (section a-a, b-b and c-c of the geometry) measured from the inlet at distance 0.4m, 0.8m and 1.4m respectively within the test section. From the Fig. 12, it is found that for a fixed temperature and inflow water velocity, the dominant frequency is independent of the measurement location. The similar kind of observations were reported in [62].

Effect of steam-water differential pressure on dominant frequency has been shown in Fig. 13. The frequency spectrum in this figure has been developed when water at 40 ℃ (313.15K) is injected into steam filled section at 600 kPa.

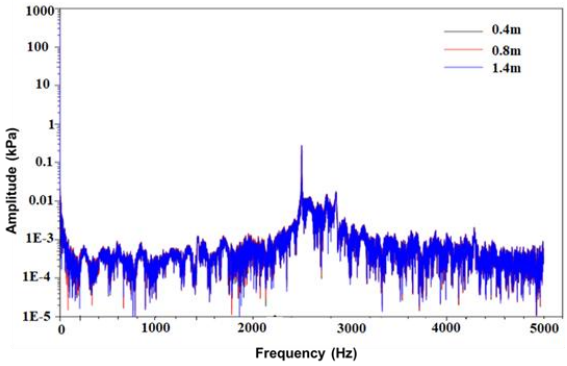

Fig. 12. Frequency spectrums of pressure oscillations at different locations within the test section.

Simulations have been performed for four different steam-water differential pressure of 400, 600, 800 and 1000 kPa . The plots in Fig. 13 show that dominant frequency occurs at at lower values of frequency i.e. 0-11 Hz. This oscillation frequency range (0-11 Hz) agreed well with the previous published researches [24, 43, 45] during CIWH condition.

From Fig. 13(a-d), it has also been observed that when the steam-water differential pressure and steam pressure is in the range of 400-800 kPa, there are two dominant frequencies in the frequency spectrums as shown in Fig. 13 (a-c). However, when steam-water differential pressure was low (ΔP=200 kPa), there is only one dominant frequency found as indicated in Fig. 13 (d). The dominant frequency is about ~1 Hz and its amplitude is about 1.93 kPa. It has been inferred that when the steam pressure is increased for a constant water pressure, the steam-water differential pressure is reduced and less agitation is produced in the test section. Consequently, the oscillations produced are low in intensity than observed in the case of smaller differential pressure.

Fig. 14 shows the relationship between peak amplitude of dominant frequencies with the steam-water differential pressure in the range of~ 400-1000 kPa. The maximum amplitude of first dominate frequency is found higher than peak value of second dominant

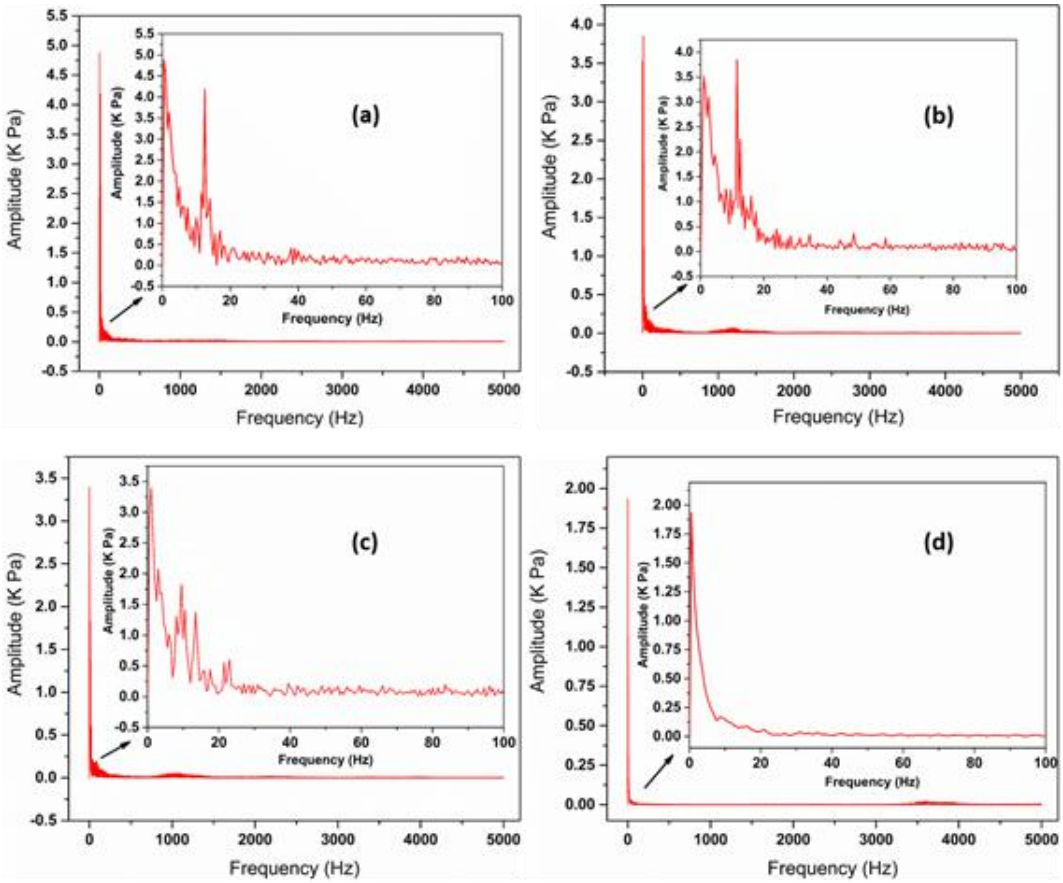

Fig. 13.Frequency spectrums of pressure oscillations against injected water at 40 ℃ and 1200 kPa for different steam pressure (a) 400 kPa (b) 600 kPa (c) 800 kPa (d) 1000 kPa

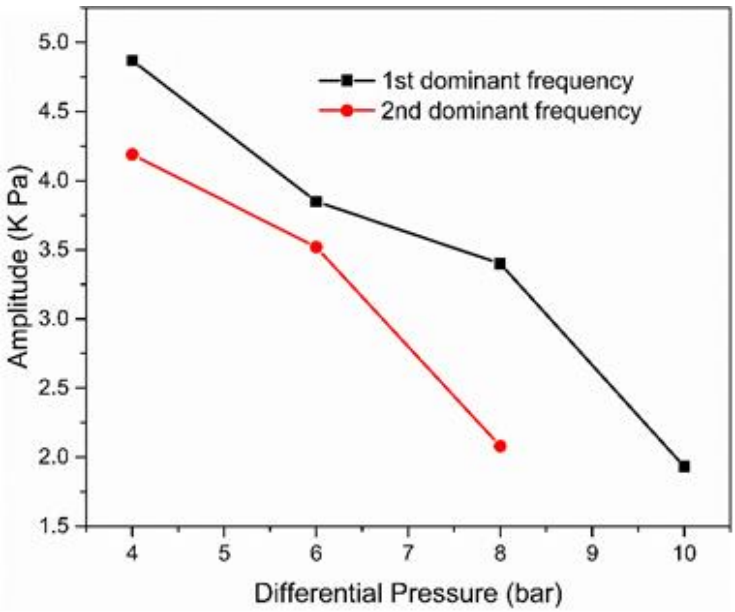

Fig. 14. Variation of amplitude of dominate frequencies with steam-water differential pressure

frequency. These results also reveal that as the differential pressure between injected water and steam increases then both the dominant frequencies have decreasing trend. This may be due to possible reason that when the steam-water differential pressure is relatively high (400-800 kPa), the injected water causes more agitation in steam section. Thus, the amplitude of dominant frequency decreases with the increasing steam-water differential pressure as shown in Fig. 14. This injection of water causes growth and propagation of the interface wave. Thus interfacial instability also occurs due to Kelvin–Helmholtz instabilities [5, 55, 56]. As a result of this vigorous mixing, steam pocket are generated within the test section which needs some additional time to be condensed. The condensation of these steam pockets causes the appearance of second dominant frequency.

The first dominant frequency, as stated earlier is the frequency with smaller frequency as compared to second dominant frequency which has larger value. As the first frequency in this range closely matches with natural frequency of the fluid domain and may resonate. Due to possibility of resonance, first dominant frequency has gained deep concern in the DCC process. However, the second dominant frequency also become important in certain transient conditions.

4.5.1 Effect of degree of steam superheating on dominant frequency pressure peak

The frequency spectrogram for pressure oscillations due to change in degree of steam superheating is shown in Fig.15(a-c) From these figure, it can be inferred that frequency and amplitude of the dominant frequency is almost independent from effects of the steam superheating. With the change in degree of steam superheating only negligible variations exist in frequency spectrum. As mentioned earlier, these minor effects may arise from the variation in local conditions of temperatures and pressure for various degree of steam superheating.

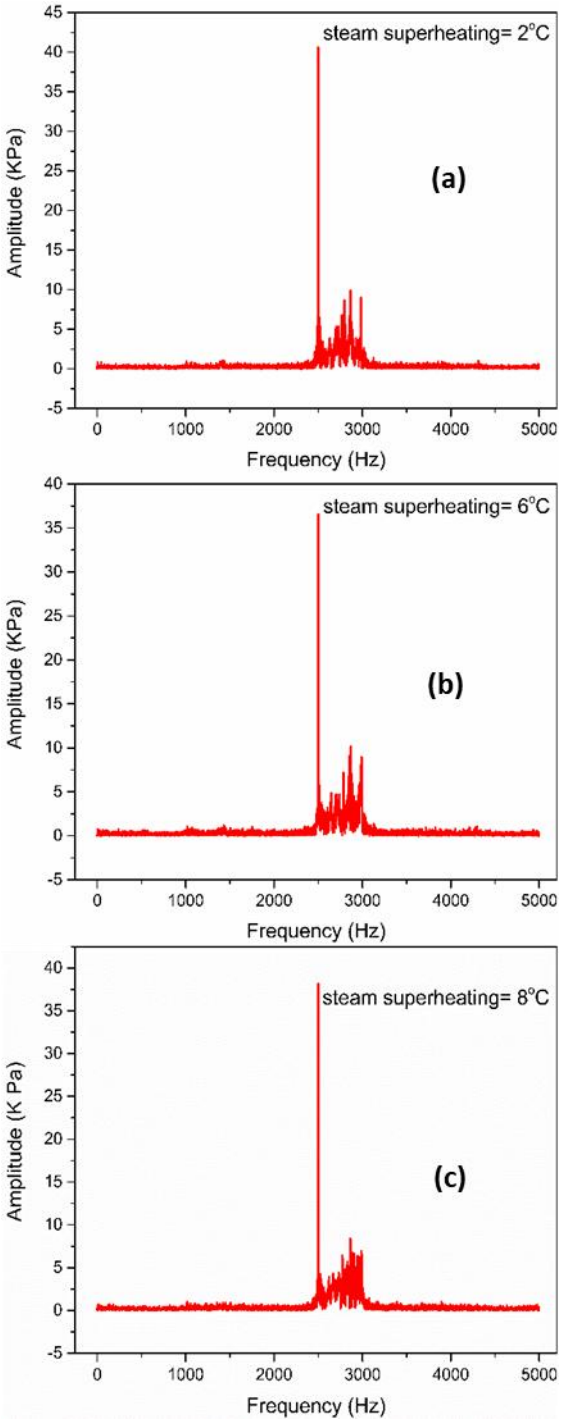

Fig.15. Frequency spectrograms for pressure oscillations single at various degree of steam superheating (a) 2^{o} C (b) 4^{o} C (c) 6^{o} C.

4.5.2 Effect of velocity on dominant frequency pressure peak

Fig. 16 and Fig. 17 shows the frequency spectrums of pressure oscillations for two different injecting water velocity values of 1m/s and 5m/s, respectively. For each velocity, effects from five different water temperatures i.e. 20, 30, 40, 50 and 60 ℃ have been studied. From Fig. 16, the first and second dominant frequency has been found as 0.5Hz and 2500 Hz, respectively. It has been found that at injecting water velocity of 1m/s, the dominant frequency has not noticeable effect with water temperature. In Fig. 17 multiple dominant frequency peaks have been observed. The first dominant frequency has been found in the range of 1415-1435 Hz while second dominant frequency as 2855-2983 Hz. It is noteworthy that the both dominant frequency decreases with the water temperature. This might be due to the fact that condensation potential of water decreases with water temperature. As a result, the collapsing of number of steam pockets from condensation phenomenon decreases. In Fig. 17 multiple dominant frequency peaks appears near second dominant frequency. The frequency band width of these peaks becomes narrow with water temperature due to reduce condensation capability of water.

The value second dominant frequency has been observed greater in value than the first dominant frequency. Although the values of these frequencies are higher and safer under normal operating conditions. However, these higher values may be harmful for system integrity when it becomes comparable to natural frequency of the fluid domain under certain accidental conditions [11]. For such scenario, the importance of such higher value frequency in general and second dominant frequency in particular becomes significant. Usually the first dominant frequency for CIWH lies in the range of 0-50Hz [24, 43] as seen in Fig. 13.However, in previous published literature, some cases have been reported where first and or second dominant frequency during pressure oscillations had exceeded this range [13, 21, 24, 42, 62]. It has been noted that with the increase in the velocity of the injected water, the amplitude of the pressure increases. This is due to earlier said reason that the imparted momentum increases with the injection velocity which causes amplitude to grow higher. Similarly, the turbulent nature of the flow within the test section strengths with the increase in injection water velocity. This enhances the mixing of steam-water and the disturbance within the interfacial wave grows causing the more oscillations frequency which can be seen in Fig. 17 Therefore, at same temperature but different velocity values, the intensity of pressure oscillations in Fig. 17 (e) is stronger than oscillations in Fig. 16 (e).

The effect of injected water velocity and its temperature on amplitude of dominant frequencies has been summarized in Fig. 18. From this figure, it is clear that at the pressure amplitudes for higher velocity are larger than observed with lower velocity values. Similarly, for the given constant velocity conditions, second dominate frequency has larger amplitude than first dominant frequency. For smaller injected water velocity of 1m/s, the change in amplitude value for both first and second dominant frequency has a little effect. For water injecting velocity of 3m/s, the amplitude of first dominant frequency first decreased up to water temperature of 40 ℃ and then increased. Similar kind of trends were observed for both first and second dominant frequency for case of water velocity of 5m/s. The trend for amplitude of second dominant frequency for water injection velocity of 3m/s almost remained stable yet had changing effect around water temperature of 40 ℃. At higher temperature 40^{o}C-60^{o}C, the condensation capability within the test section decreases resulting in stable interface wave with lower frequency and higher-pressure amplitude. It is also found that at a constant temperature, the pressure amplitude increased with the increase in water injecting velocity. The higher the velocity of the injected water, more the momentum was imparted into the steam domain resulting in stronger pressure amplitude. Moreover, when the higher velocity is, the interfacial waves merges and lesser

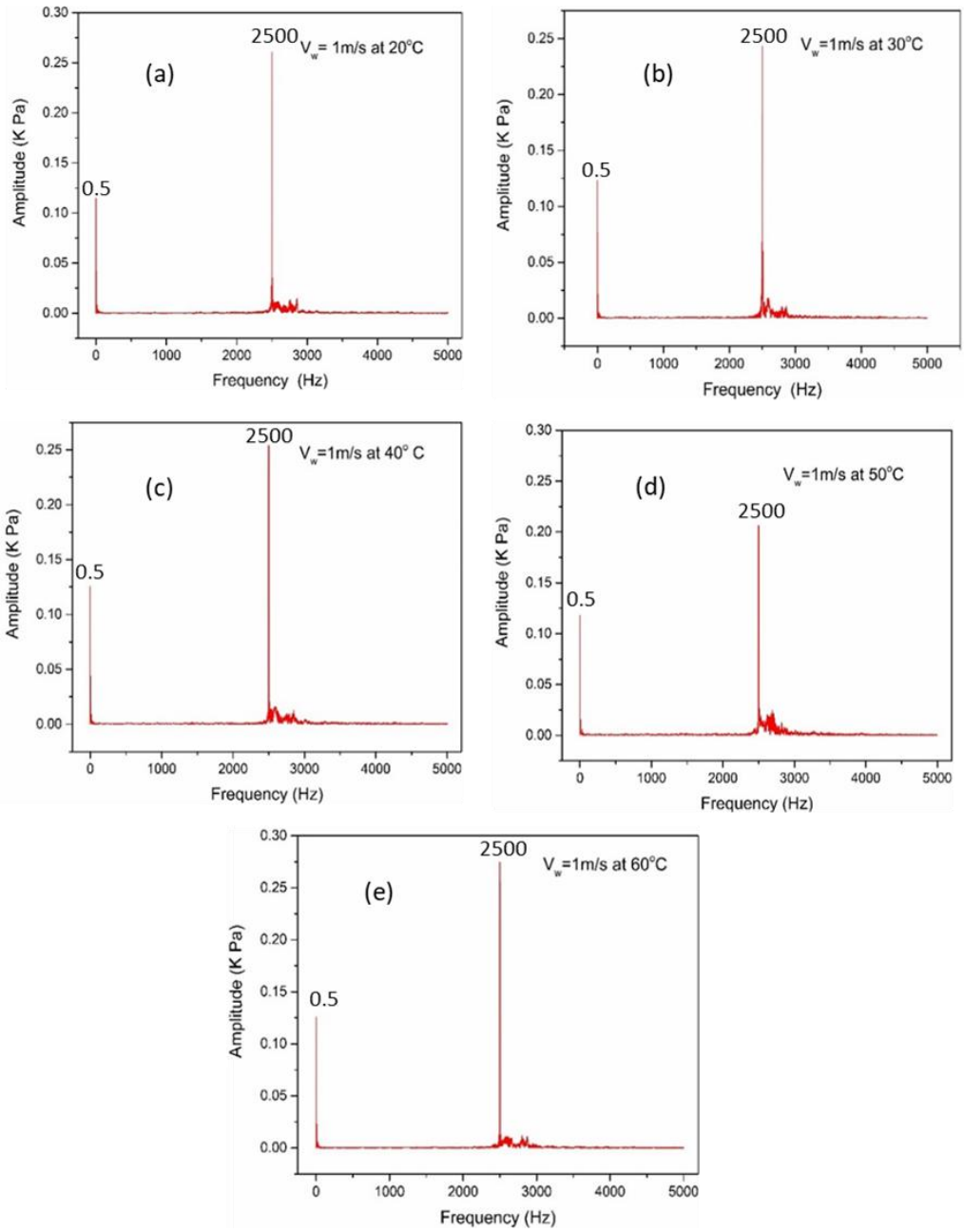

Fig. 16. Frequency spectrums of pressure oscillations within the test section for water injecting velocity of 1m/s at various temperatures, (a) 20 ℃ (b) 30 ℃(c) 40 ℃ (d) 50 ℃ (e) 60 ℃

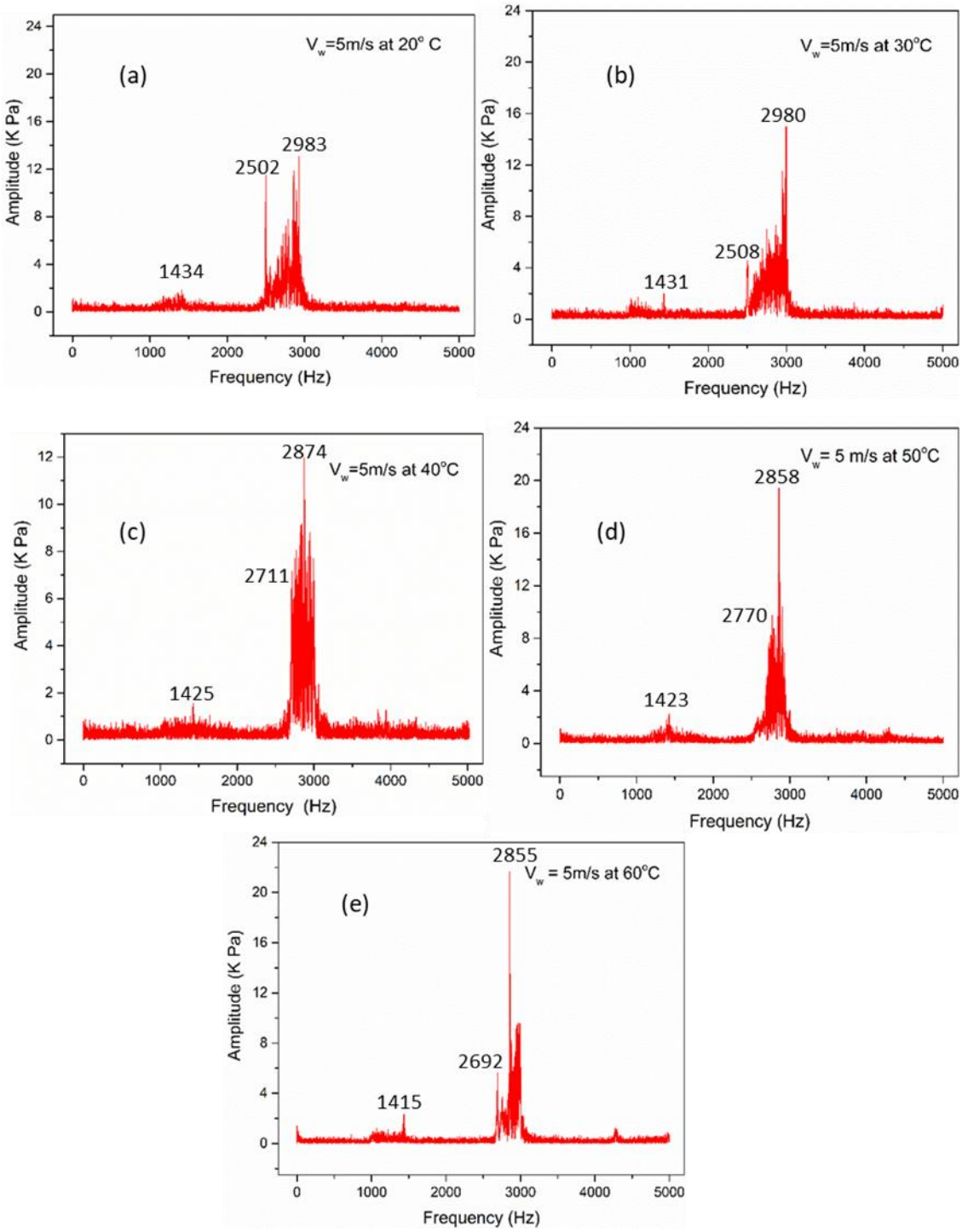

Fig. 17. Frequency spectrums of pressure oscillations within the test section for water injecting velocity of 5m/s at various temperatures, (a) 20 ℃ (b) 30 ℃(c) 40 ℃ (d) 50 ℃ (e) 60 ℃

oscillations frequency with stronger the is produced [63]. A large pressure amplitude also found when the injected water velocity was higher at elevated temperature, i.e., maximum value of 21.65 kPa was observed with water velocity of 5m/s at 60 ℃. Furthermore, at higher water temperatures, the condensation capability of the steam decreases, the steam pocket takes longer time to be condensed reducing condensation frequency. The reduction in frequency causes the amplitude of the pressure to be high.

4.5.3 Dominant frequency regime map

From the above investigation of steam-water frequency spectrum under different condition, it has been observed that sometime only one dominant frequency appears and sometimes two dominant frequencies have been noticed for certain operating Fig. 19 shows dominant frequency regime map for steam-water DCC has been proposed based on the pressure of the steam and water. In this regime map, numbers of dominant frequencies have been recorded for the given steam pressure 500-1000 kPa and steam-water differential pressure of 200-800 kPa. The frequency spectrum has only one dominant frequency in the range of steam pressure 5-10 bar and steam-water differential pressure of 200kPa. Similarly, one dominant frequency is obtained when steam pressure, P steam = 500kPa with steam-water differential pressure in the range of ΔP =200-600 kPa. This dominate frequency results from oscillations of the main steam section when the injection of the spray water is not vigorous. However, when the steam pressure was P steam $\geq$ 600 kPa and steam-water differential pressure ΔP $\geq$ 400 kPa, the pressure oscillations have two dominant frequencies. One later case has also been observed for P steam =500 kPa & ΔP =800 kPa. When either the injected water pressure was high i.e. ΔP $\geq$ 600 or steam pressure P steam $\geq$ 600 kPa, steam condenses and large steam pockets zone are condensed and ruptured within the test section. So, two dominant frequencies have been observed in the pressure oscillations under these conditions. Thus, the study of pressure oscillations characteristics and impact of dominant frequencies is very critical for avoidance of the resonance phenomenon.

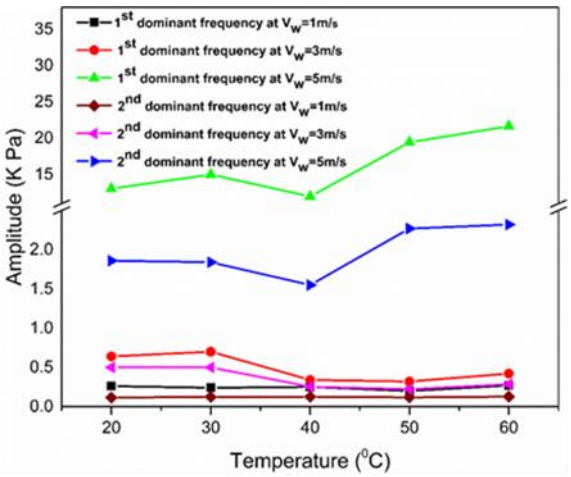

Fig. 18 . Comparison in amplitudes of dominant frequencies at different water injection velocities.

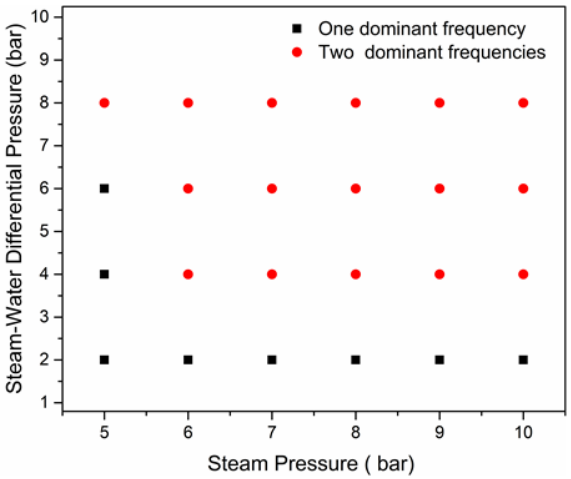

Fig. 19 Dominant frequency map for steam pressure against steam-water differential pressure

5. Conclusions

In the present work, the pressure oscillations characteristics and their dominant frequencies during steam-water DCC have been investigated by injecting subcooled water into steam filled horizontal pipe. Various operating conditions have been considered by

varying velocity, temperature, and pressure values of either water or steam. The major conclusions have been summarized as under:

(1)- A large instantaneous pressure spike appears near the water inlet section of the pipe. The magnitude of this peak increases with water injecting velocity but has no noticeable effect from water temperature.

(2)- With the increase in water injecting velocity, the transition from stratified flow condition to slug flow is shifted upstream causing early start of pressure oscillations. The strength of pressure oscillations increases with velocity.

(3)- The expansion and compression waves during pressure oscillations depends on steam-water differential pressure in the pipe. With the increase in differential pressure, the increase in peak temperature and decrease in valley temperatures within the test sections is observed.

(4)- The effects of degree of steam superheating on pressure oscillations is negligible.

(5)- The dominant frequency during pressure oscillations within pipe is independent of measurement locations. The frequency spectrum has only one dominant frequency in the range of steam pressure 500-1000 kPa and steam-water differential pressure of 200 kPa. Similarly, one dominant frequency has been observed when steam pressure was P_{steam} = 500 kPa with steam-water differential pressure in the range of 2-6 bar. However, when the steam pressure was $P_{steam} \geq 600$ kPa and steam-water differential pressure $\Delta P \geq 400$ kPa, the pressure oscillations have two dominant frequencies. Both frequencies have decreasing trend with increase in steam-water differential pressure. The second frequency disappeared as differential pressure is reduced to 200 kPa.

(6)- At water injecting velocity of 3-5m/s, the increase in water temperature causes initially a decrease and then in the first and second dominant frequencies. At lower water velocity of 1m/s, the first dominant frequency does not change significantly with increase in subcooled water temperature.

Acknowledgment

This present work was supported by Higher Education Commission, Govt. of Pakistan under grant, HEC indigenous PhD fellowship scheme (417-47877-2EG4-042). The authors acknowledge the supports.

Conflict of interest

The Authors declare no potential conflicts of interest with respect to the research, authorship, and/or publication of this article.

References

[1] P. Datta, A. Chakravarty, K. Ghosh, A. Mukhopadhyay, and S. Sen, "Direct Contact Condensation of Steam in Subcooled Water," in *Two-Phase Flow for Automotive and Power Generation Sectors*: Springer, 2019, pp. 337-362.

[2] S. Dirndorfer, "Steam condensation induced water hammer in a vertical up-fill configuration within an integral test facility: experiments and computational simulations," Universitätsbibliothek der Universität der Bundeswehr München, 2017.

[3] S. Song, X. Yue, Q. Zhao, D. Chong, W. Chen, and J. Yan, "Numerical study on mechanism of condensation oscillation of unstable steam jet," *Chemical Engineering Science*, vol. 211, p. 115303, 2020.

[4] Q. Yang, B. Qiu, W. Chen, D. Chong, J. Liu, and J. Yan, "Experimental investigation on the condensation regime and pressure oscillation characteristics of vertical upward steam jet condensation with low mass flux," *Experimental Thermal and Fluid Science*, vol. 111, p. 109983, 2020.

[5] P. Datta *et al.*, "A numerical analysis on the effect of inlet parameters for condensation induced water hammer," *Nuclear Engineering and Design*, vol. 304, pp. 50-62, 2016.

[6] J. Sun, X. Ran, Z. Zhang, X. Cao, G. Fan, and M. Ding, "Effects of direct contact condensation on flow characteristics of natural circulation system at low pressure," *Frontiers in Energy Research*, vol. 8, p. 173, 2020.

[7] L. Štrubelj, G. Ézsöl, and I. Tiselj, "Direct contact condensation induced transition from stratified to slug flow," *Nuclear engineering and design*, vol. 240, no. 2, pp. 266-274, 2010.

[8] D. Chong, X. Yue, L. Wang, Q. Zhao, and J. Yan, "Experimental investigation on the condensation patterns and pressure oscillation characteristics of steam submerged jet through a horizontal pipe at low steam mass flux," *International*

Journal of Heat and Mass Transfer, vol. 139, pp. 648-659, 2019.

[9] C. Urban and M. Schlüter, "Investigations on the stochastic nature of condensation induced water hammer," *International journal of multiphase flow*, vol. 67, pp. 1-9, 2014.

[10] F. Yuan, D. Chong, Q. Zhao, W. Chen, and J. Yan, "Pressure oscillation of submerged steam condensation in condensation oscillation regime," *International Journal of Heat and Mass Transfer*, vol. 98, pp. 193-203, 2016.

[11] B. Qiu, J. Yan, J. Liu, D. Chong, Q. Zhao, and X. Wu, "Experimental investigation on the second dominant frequency of pressure oscillation for sonic steam jet in subcooled water," *Experimental thermal and fluid science*, vol. 58, pp. 131-138, 2014.

[12] D. Chong, Q. Zhao, F. Yuan, Y. Cong, W. Chen, and J. Yan, "Experimental and theoretical study on the second dominant frequency in submerged steam jet condensation," *Experimental Thermal and Fluid Science*, vol. 68, pp. 744-758, 2015.

[13] Q. Zhao, W. Chen, L. Wang, D. Chong, and J. Yan, "Experimental investigation on pressure oscillations of steam jet condensation through multi-holes," *International Journal of Heat and Mass Transfer*, vol. 132, pp. 662-670, 2019.

[14] C. Chan and C. Lee, "A regime map for direct contact condensation," *International Journal of Multiphase Flow*, vol. 8, no. 1, pp. 11-20, 1982.

[15] S. J. Hong, G. C. Park, S. Cho, and C.-H. Song, "Condensation dynamics of submerged steam jet in subcooled water," *International journal of multiphase flow*, vol. 39, pp. 66-77, 2012.

[16] I. Aya, M. Kobayashi, and H. Nariai, "Pressure and fluid oscillations in vent system due to steam condensation,(II) high-frequency component of pressure oscillations in vent tubes under at chugging and condensation oscillation," *Journal of Nuclear Science and Technology*, vol. 20, no. 3, pp. 213-227, 1983.

[17] I. Aya, H. Nariai, and M. Kobayashi, "Pressure and fluid oscillations in vent system due to steam condensation,(I) Experimental results and analysis model for chugging," *Journal of Nuclear Science and Technology*, vol. 17, no. 7, pp. 499-515, 1980.

[18] S. Fukuda, "Pressure variations due to vapor condensation in liquid,(2)," *Nippon Genshiryoku Gakkai-Shi*, vol. 24, no. 6, pp. 466-474, 1982.

[19] Q. Zhao, W. Chen, F. Yuan, W. Wang, D. Chong, and J. Yan, "Pressure oscillation and steam cavity during the condensation of a submerged steam jet," *Annals of Nuclear Energy*, vol. 85, pp. 512-522, 2015.

[20] B. Qiu, J. Yan, D. Chong, and S. T. Revankar, "Experimental investigation on the mechanism of pressure oscillation for steam jet in stable condensation region," *Experimental Thermal and Fluid Science*, vol. 82, pp. 1-7, 2017.

[21] W. Chen, Q. Zhao, Y. Wang, P. K. Sen, D. Chong, and J. Yan, "Characteristic of pressure oscillation caused by turbulent vortexes and affected region of pressure oscillation," *Experimental Thermal and Fluid Science*, vol. 76, pp. 24-33, 2016.

[22] S. Cho, C. H. Song, C. K. Park, S. K. Yang, and M. K. Chung, "Experimental study on dynamic pressure pulse in direct contact condation of steam jets discharging into subcooled water," in *Proceedings of the 1st Korea-Japan Symposium on Nuclear Thermal Hydraulics and Safety, Pusan, Korea*, 1998, pp. 21-24.

[23] L. Wang, X. Yue, D. Chong, W. Chen, and J. Yan, "Experimental investigation on the phenomenon of steam condensation induced water hammer in a horizontal pipe," *Experimental Thermal and Fluid Science*, vol. 91, pp. 451-458, 2018.

[24] J. Wang, T. Lu, J. Deng, Y. Liu, Q. Lu, and Z. Zhang, "Experimental investigation on pressure oscillation induced by steam lateral injection into water flow in a horizontal pipe," *International Journal of Heat and Mass Transfer*, vol. 148, p. 119024, 2020.

[25] I. F. Barna, A. R. Imre, G. Baranyai, and G. Ézsöl, "Experimental and theoretical study of steam condensation induced water hammer phenomena," *Nuclear Engineering and Design*, vol. 240, no. 1, pp. 146-150, 2010.

[26] H. Liang, B. Zhao, C. Huang, H. Song, and X. Jiang, "Numerical simulation study on performance optimization of desuperheater," *Energy Reports*, vol. 7, pp. 2221-2232, 2021.

[27] S. K. Shukla, A. N. Samad, and S. Ghosh, "CFD simulation of steam condensation in

a subcooled water pool," *Thermal Science and Engineering Progress*, vol. 2, pp. 80-86, 2017.

[28] J. Weimer, G. Faeth, and D. Olson, "Penetration of vapor jets submerged in subcooled liquids," *AIChE Journal*, vol. 19, no. 3, pp. 552-558, 1973.

[29] D. Chong, L. Wang, W. Liu, Z. Wang, and J. Yan, "Characteristics of entrapped bubbles of periodic condensation-induced water hammer in a horizontal pipe," *International Journal of Heat and Mass Transfer*, vol. 152, p. 119534, 2020.

[30] A. Shah, I. R. Chughtai, and M. H. Inayat, "Numerical simulation of direct-contact condensation from a supersonic steam jet in subcooled water," *Chinese Journal of Chemical Engineering*, vol. 18, no. 4, pp. 577-587, 2010.

[31] L. Zhou, L. Wang, D. Chong, J. Yan, and J. Liu, "CFD analysis to study the effect of non-condensable gas on stable condensation jet," *Progress in Nuclear Energy*, vol. 98, pp. 143-152, 2017.

[32] L. Wang, X. Yue, Q. Zhao, D. Chong, and J. Yan, "Numerical investigation on the effects of steam and water parameters on steam jet condensation through a double-hole nozzle," *International Journal of Heat and Mass Transfer*, vol. 126, pp. 831-842, 2018.

[33] P. Datta, A. Chakravarty, K. Ghosh, A. Mukhopadhyay, and S. Sen, "Modeling of steam–water direct contact condensation using volume of fluid approach," *Numerical Heat Transfer, Part A: Applications*, vol. 73, no. 1, pp. 17-33, 2018.

[34] L. Strubelj and I. Tiselj, "Condensation of the steam in the horizontal steam line during cold water flooding," in *International Conference on Nuclear Energy for New Europe*, 2006, pp. 18-21.

[35] H. Ding, Y. Luo, and X. Yuan, "Numerical investigation of heat transfer in direct contact condensation of steam to subcooled water spray," *Chemical Engineering and Processing-Process Intensification*, vol. 140, pp. 52-63, 2019.

[36] F. He, J. Yang, and X. Wang, "Condensation-induced steam bubble collapse in a pipeline," *Tsinghua science and technology*, vol. 5, no. 4, pp. 424-427, 2000.

[37] G. Patel, V. Tanskanen, and R. Kyrki-Rajamäki, "Numerical modelling of low-Reynolds number direct contact condensation in a suppression pool test facility," *Annals of Nuclear Energy*, vol. 71, pp. 376-387, 2014.

[38] I. Ansys, "ANSYS FLUENT theory guide," *Canonsburg, Pa*, p. 794, 2011.

[39] X. Chen, M. Tian, X. Qu, and Y. Zhang, "Numerical investigation on the interfacial characteristics of steam jet condensation in subcooled water flow in a restricted channel," *International Journal of Heat and Mass Transfer*, vol. 137, pp. 908-921, 2019.

[40] A. Shah, I. R. Chughtai, and M. H. Inayat, "Experimental and numerical analysis of steam jet pump," *International journal of multiphase flow*, vol. 37, no. 10, pp. 1305-1314, 2011.

[41] S. Patankar, *Numerical heat transfer and fluid flow*. CRC press, 2018.

[42] Q. Xu, W. Liu, W. Li, T. Yao, X. Chu, and L. Guo, "Experimental investigation on interfacial behavior and its associated pressure oscillation in steam jet condensation in subcooled water flow," *International Journal of Heat and Mass Transfer*, vol. 145, p. 118779, 2019.

[43] S. Li, W. Han, T. Lu, L. Feng, N. Hou, and T. Li, "Numerical study on oscillation characteristics of large chugging of direct condensation of steam in a Tee junction with flowing sub-cooled water," *Progress in Nuclear Energy*, vol. 135, p. 103720, 2021.

[44] X.-p. Yang, J. Liu, J.-p. Liu, N.-n. Chen, and J.-j. Yan, "Interface dynamics and pressure oscillation of stable steam jet condensation in water flow in a confined channel with the presence of non-condensable gas," *International Journal of Heat and Mass Transfer*, vol. 111, pp. 1157-1171, 2017.

[45] W. Li, Z. Meng, J. Wang, J. Liu, and Z. Sun, "Experimental investigations on pressure oscillation induced by steam-air mixture gas sonic jets in subcooled water," *International Journal of Heat and Mass Transfer*, vol. 128, pp. 450-458, 2019.

[46] S. Li, P. Wang, and T. Lu, "CFD based approach for modeling steam–water direct contact condensation in subcooled water flow in a tee junction," *Progress in Nuclear Energy*, vol. 85, pp. 729-746, 2015.

[47] A. Quddus, A. Shah, K. R. Qureshi, A. Tahir, M. Iqbal, and M. K. Ayub, "Numerical study on pressure oscillations amplitude distribution induced by water

flow into pipe filled with steam," *Annals of Nuclear Energy*, vol. 172, p. 109095, 2022.

[48] A. Quddus, A. Shah, K. R. Qureshi, M. K. Ayub, M. Iqbal, and A. J. K. Samee, "Computational study of subcooled water injection into steam line: effect of Reynolds number on flow transition to study condensation induced water hammers," 2022.

[49] R. Szijártó, A. Badillo, B. Ničeno, and H.-M. Prasser, "Condensation models for the water–steam interface and the volume of fluid method," *International Journal of Multiphase Flow*, vol. 93, pp. 63-70, 2017.

[50] A. Kaliatka, E. Uškuras, and M. Vaišnoras, "RELAP5 code analysis of water hammer wave behavior," *Power Engineering, Lithuanian Academy of Sciences, Vilnius*, vol. 4, pp. 1-9, 2005.

[51] P. Datta *et al.*, "Modeling and analysis of condensation induced water hammer," *Numerical Heat Transfer, Part A: Applications*, vol. 74, no. 2, pp. 975-1000, 2018.

[52] W. H. Lee, "A pressure iteration scheme for two-phase modeling," *Los Alamos Scientific Laboratory, Los Alamos, NM, Report No. LA-UR*, pp. 79-975, 1979.

[53] M. Simpson and C. Chan, "Hydrodynamics of a subsonic vapor jet in subcooled liquid," 1982.

[54] S. Sukamta and T. A. R. Purnomo, "Experimental Investigation of slugging as initiating water hammer phenomena through indirect contacts steam condensing in a horizontal pipe heat exchanger," *International Journal of Technology*, vol. 6, no. 6, 2015.

[55] A. Khan, N. U. Haq, I. R. Chughtai, A. Shah, and K. Sanaullah, "Experimental investigations of the interface between steam and water two phase flows," *International Journal of Heat and mass transfer*, vol. 73, pp. 521-532, 2014.

[56] P. G. Drazin and W. H. Reid, *Hydrodynamic stability*. Cambridge university press, 2004.

[57] M.-H. Chun and S.-O. Yu, "Effect of steam condensation on countercurrent flow limiting in nearly horizontal two-phase flow," *Nuclear Engineering and Design*, vol. 196, no. 2, pp. 201-217, 2000.

[58] G. Celata, M. Cumo, G. Farello, and G. Focardi, "Direct contact condensation of superheated steam on water," *International journal of heat and mass transfer*, vol. 30, no. 3, pp. 449-458, 1987.

[59] X. Yang, P. Fu, N. Chen, Y. Zhou, J. Liu, and J. Wei, "Experimental study on pressure pulse generated by condensing subsonic/supersonic steam jet in a horizontal channel," *Nuclear Engineering and Design*, vol. 378, p. 111175, 2021.

[60] I. F. Barna and G. Ezsöl, "Multiple condensation induced water hammer events, experiments and theoretical investigations," *Kerntechnik*, vol. 76, no. 4, pp. 231-236, 2011.

[61] H.-M. Prasser, G. Ezsol, G. Baranyai, and T. Suhnel, "Spontaneous water hammers in a steam line in the case of cold water ingress," *Multiphase Science and Technology*, vol. 20, no. 3-4, 2008.

[62] B. Qiu, S. Tang, J. Yan, J. Liu, D. Chong, and X. Wu, "Experimental investigation on pressure oscillations caused by direct contact condensation of sonic steam jet," *Experimental thermal and fluid science*, vol. 52, pp. 270-277, 2014.

[63] X. Yang, P. Fu, N. Chen, J. Liu, and J. Wei, "Mechanisms of pressure pulse for condensing supersonic steam jet in a rectangular channel," *Experimental Thermal and Fluid Science*, vol. 105, pp. 223-233, 2019.

[64] W. Chen, Y. Wang, Q. Zhao, D. Chong, and J. Yan, "Experimental investigation on the second dominant frequency of supersonic steam jet condensation oscillation and its propagation characteristic," *Annals of Nuclear Energy*, vol. 97, pp. 122-131, 2016.